

Simulation, Measurement, and Parameter Extraction for a 5.8 GHz Negative Permittivity Metamaterial

Thomas P. Weldon, Konrad Miehle, Ryan S. Adams, and Kasra Daneshvar

Department of Electrical and Computer Engineering

University of North Carolina at Charlotte

Charlotte, NC 28223, USA

Email: tpweldon@uncc.edu

Abstract—Metamaterials are commonly comprised of ring structures with negative effective permeability and wire structures with negative effective permittivity. However, the catalog of available negative permittivity devices remains somewhat limited. Recently, a novel unit cell comprised of two disks connected by a metal post was presented. The analysis of the unit cell predicted a resonant response, with negative effective permittivity above the resonant frequency. To verify the predicted metamaterial behavior, an experimental prototype has been fabricated and the effective permittivity has been extracted using measured S-parameters. The experimental results for the prototype device show the predicted resonant behavior, and the extracted parameters show a region of negative permittivity above resonance.

I. INTRODUCTION

Although there has been considerable progress in the design of metamaterials for a wide range of potential applications, the development of new unit cell structures continues to be an area of active research. [1]–[4] In this, the range of available negative permittivity and negative permeability structures remains somewhat limited. Furthermore, the focus on magnetic structures by early investigators may offer some unexplored opportunities in the development of negative-permittivity structures.

To explore such opportunities, the analysis of a negative effective permittivity unit cell has recently been presented for a device comprised of a central inductive post terminated by two discs [5]. The approach is based on Ampere’s circuital law and the Maxwell-Ampere equation in a way that naturally describes the coupling of the electromagnetic field to the resonant structure. The results from Ampere’s law are then used to compute the dipole moment of the unit cell and to derive effective permittivity using polarization [6]. This straightforward analysis leads to a simple expression for the negative effective permittivity of the unit cell as a function of frequency, with resonant behavior that is similar to that of split ring resonators [4]. Thus, the approach provides more direct insight into the interaction of the device with the electromagnetic field than may be offered by circuit-based approaches [7]. The remainder of this article expands upon the development outlined in [5] and further includes measured and simulated results for an experimental prototype.

In the following section, the analysis of the negative-permittivity structures is reviewed. The behavior of magnetic

resonators are first outlined, to show the similarities between the theoretical development and results for the electric resonator and magnetic resonator. Finally, simulation and experimental results are given for a prototype, with negative permittivity demonstrated just above the 5.8 GHz resonant frequency of the device.

II. ANALYSIS

Before reviewing the analysis of the negative permittivity device, it is helpful to briefly review the more common split ring resonator, since it follows a similar development. First, the effective permeability of the split ring resonator is derived from magnetic dipole moment and macroscopic magnetization. Then, the effective permittivity of the electric resonator is derived from electric dipole moment and polarization. Thus, the analysis of a split ring resonator provides a similar framework to the analysis of the negative-permittivity metamaterials to follow [4], [8]–[11]. As usual, the dimensions of the unit cell are taken to be less than 10 percent of a wavelength, so that the incident magnetic field is uniform over the unit cell.

For simplicity, consider a single split-ring resonator (SSRR) as illustrated in Fig. 1. It is fairly straightforward to show that the structure exhibits negative effective permeability near resonance, where the resonant frequency is set by the inductance of the metal ring and capacitance of the gap in the ring. The current in the ring gives rise to a magnetic dipole moment in the SSRR of $\mathbf{m} = i_r A_R$, with macroscopic magnetization \mathbf{M} being determined as the magnetic dipole moment per unit volume [3]–[5]:

$$\mathbf{M} = \frac{i_r A_R}{l_x l_y l_z} = -\mu_0 \mathbf{H}_0 \frac{A_R^2}{l_x l_y l_z} \frac{s^2 C_g}{1 + s^2 L_R C_g}, \quad (1)$$

and where the dimensions of the unit cell comprising this magnetic metamaterial particle are l_x , l_y , and l_z , the split ring has an area A_R , the current in the split ring is i_r , the incident magnetic field is \mathbf{H}_0 , C_g is the capacitance of the gap, L_R is the self-inductance of the SSRR, and s is the Laplace complex angular frequency.

Since $\mathbf{M} = \chi_m \mathbf{H}$ and $\mu_r = 1 + \chi_m$, it follows that

$$\mu_r = 1 + \frac{\mu_0 A_R^2}{l_x l_y l_z} \frac{\omega^2 C_g}{1 - \omega^2 L_R C_g}, \quad (2)$$

where χ_m is the magnetic susceptibility, the permeability of free space is $\mu_0 = 1.26 \times 10^{-6}$ H/m, ω is angular frequency

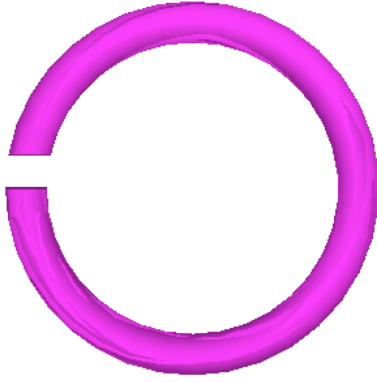


Fig. 1. Illustration of an example of a single split-ring resonator (SSRR) used to create negative effective permittivity near resonance. The area of the metal ring is A_R , with an air gap in the ring as illustrated.

in rad/s, and μ_r is the effective relative permeability of the metamaterial. Commonly, this is expressed as:

$$\mu_r = 1 + \frac{\mu_0 A_R^2}{L_R l_x l_y l_z} \frac{\omega^2}{\omega_m^2 - \omega^2}, \quad (3)$$

where $\omega_m = 1/\sqrt{L_R C_g}$ is the magnetic resonance frequency [5], [11]. The resulting expression in (3) for μ_r forms the basis for such negative-permeability metamaterials, where μ_r becomes a large negative value at frequencies where the denominator $\omega_m^2 - \omega^2$ is a small negative number [4].

Just as the the split ring resonator was analyzed above for negative-permeability metamaterials, a similar analysis is now given for the negative-permittivity metamaterials under consideration [5]. Consider the electric disk resonator (EDR) in Fig. 2, resembling a three-dimensional version of the I-shaped structures in [6] and [12]. The dimensions of the unit cell comprising this electric metamaterial particle are the same as the magnetic component of Fig. 1, l_x , l_y , and l_z . The metal disks at the top and bottom faces of the structure have areas A_D and are connected together by a metal post with inductance L_p and length l_p . As before, the dimensions of the unit cell are taken to be less than 10 percent of a wavelength, so that the incident electric field E_0 is uniform over the unit cell. As shown in Fig. 2, the current in the post that connects the two disks is i_p , and the voltage between the upper and lower disk is v_d .

Using Ampere's circuital law, the time derivative of the electric flux at the top face of the upper disk equals the current in the post plus the time derivative of the electric flux at the bottom face of the top disk [5]:

Along the same lines as the analysis of the SSRR above, is fairly straightforward to show that the EDR of Fig. 2 exhibits negative effective permittivity near resonance, where the resonant frequency is set by the fringe capacitance between the two metal disks and the inductance of the metal post connecting the two disks [5]. The current in the charge on the two disks gives rise to an electric dipole moment in the EDR of $\mathbf{p} = ql_p \hat{\mathbf{y}}$, with the polarization \mathbf{P} being determined



Fig. 2. Electric unit cell example showing example electric disk resonator (EDR) with two brass disks connected by a cylindrical rod. The outer faces of the two metal disks at the top and bottom of the structure have areas A_D , and are connected together by a metal post with inductance L_p and length l_p .

as the electric dipole moment per unit volume [5]:

$$\mathbf{P} = \frac{\mathbf{p}}{l_x l_y l_z} = \mathbf{E}_0 \frac{C_0 l_p}{l_x l_z} \left(\frac{1}{1 + s^2 L_p C_F} \right), \quad (4)$$

where L_p is the inductance of the metal post connecting the two disks, \mathbf{E}_0 is the incident electric field, C_F is the fringe capacitance between the upper disk and the lower disk, $C_0 = \epsilon_o A_D / (l_y - l_p)$ is a capacitance-like parameter, the outer faces of the two disks have area A_D , $v_0 = E_0 l_y$ is the voltage across the full length of the unit cell, and the permittivity of free space is $\epsilon_o = 8.85 \times 10^{-12}$ F/m.

Because $\mathbf{P} = \chi_e \epsilon_o \mathbf{E}$ and $\epsilon_r = 1 + \chi_e$, it follows that

$$\epsilon_r = 1 + \mathbf{E}_0 \frac{C_0 l_p}{\epsilon_o l_x l_z} \left(\frac{1}{1 + s^2 L_p C_F} \right), \quad (5)$$

$$(6)$$

where ϵ_r is the effective relative permittivity and χ_e is the electric susceptibility,

In a similar fashion to the SSRR, the effective relative permittivity can also be expressed as

$$\epsilon_r = 1 + \mathbf{E}_0 \frac{C_0 l_p}{\epsilon_o l_x l_z} \left(\frac{\omega_e^2}{\omega_e^2 - \omega^2} \right), \quad (7)$$

where $\omega_e = 1/\sqrt{L_p C_F}$ is the electric resonance frequency. The resulting expression in (7) for ϵ_r forms the basis for the proposed negative-permittivity metamaterials, where ϵ_r becomes a large negative value at frequencies where the denominator $\omega_e^2 - \omega^2$ is a small negative number. In addition, the denominator causes a resonant narrowband response around the center frequency ω_e .

III. EDR SIMULATION AND MEASUREMENT

The EDR described in the preceding section was simulated before measuring the response of the prototype device. The simulated EDR had disks of radius 3.2 mm connected by a 5.5 mm long copper rod of diameter 0.15 mm ($l_p = 5.5$ mm and $A_D = 10.24$ mm²). As shown in the HFSS simulation results of Fig. 3, the S-parameters of the EDR in WR-187 waveguide show the predicted narrowband resonant behavior.

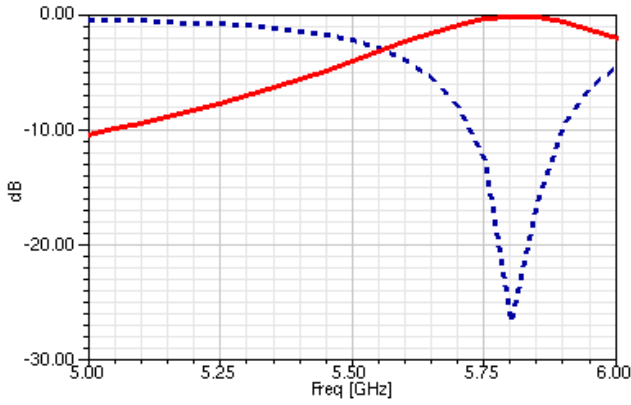


Fig. 3. HFSS simulation S-parameters of the EDR of Fig. 2 in WR-187 waveguide showing narrowband resonant behavior. Solid red line is S_{11} and dotted blue line is S_{21} .

The solid red curve of Fig. 3 shows $|S_{11}|$ from 5.0 to 6.0 GHz for the simulation, with the expected strong resonance at $\omega_e = 5.8$ GHz. The dotted blue curve shows $|S_{21}|$.

A prototype of the EDR of Fig. 2 was also fabricated, with two brass disks of radius 3.2 mm connected by a 5.5 mm long copper rod of diameter 0.15 mm ($l_p = 5.5$ mm and $A_D = 10.24$ mm²). A photograph of the measured prototype is given in Fig. 4. Measured S-parameters for the prototype of Fig. 4 are given in Fig. 5, and the results are in good agreement with the simulation of Fig. 3. The solid red curve shows measured $|S_{11}|$ from 5.0 to 6.0 GHz for the prototype, with the expected strong resonance at 5.8 GHz. The dotted blue curve shows measured $|S_{21}|$ for the prototype.

The real part of the effective permittivity of the prototype EDR of Fig. 4 was extracted using the S-parameters of Fig. 5, drawing upon common methods such outlined as [13] and [14]. Fig. 6 shows the real part of the effective permittivity $\text{Re}(\epsilon_r)$ as the solid red curve. Note that the permittivity ϵ_r is a large positive value below the 5.8 GHz resonance, and a large negative value above resonance, as predicted from (6) and (7).

Finally, the simulated electric field below resonance is shown in Fig. 7, where the top right shows the 430 V/m incident electric field in cyan arrows pointing up, and the lower right shows the EDR and the resulting 1500 V/m total electric field in red arrows pointing up. The strong reversed electric field above resonance is shown in Fig. 8, where the

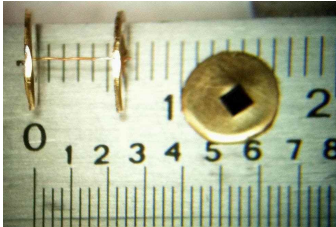


Fig. 4. Prototype electric disk resonator (EDR). The prototype EDR shown in the upper left was fabricated with two brass disks connected by a copper wire. A view of a disk is shown in the top right, with a 1.5×1.5 mm square black die shown for size reference. Upper scale is in cm.

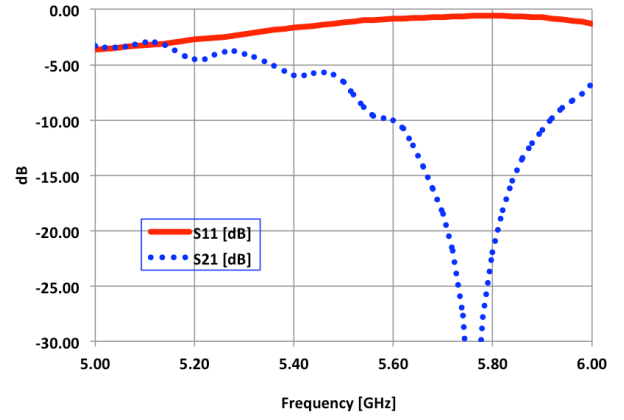


Fig. 5. Measured S-parameters of the EDR of Fig. 4 in WR-187 waveguide showing narrowband resonant behavior. Solid red line is S_{11} and dotted blue line is S_{21} .

top right shows the 430 V/m incident electric field in cyan arrows pointing up, and the lower right shows the EDR and the resulting 1500 V/m total electric field in red arrows pointing down.

IV. CONCLUSION

A straightforward unit cell analysis was presented for a device with negative effective permittivity comprised of two metal disks connected by a metal post. The coupling of the external field to the device was directly described through the Ampere circuital law, and the theoretical effective permittivity was calculated through polarization. Electromagnetic simulations of the device in HFSS confirmed the expected resonant behavior and the expected field reversals above and below resonance. Finally, measurement of a prototype device demonstrated the expected resonant behavior when tested in waveguide, with negative effective permittivity demonstrated above the resonant frequency.

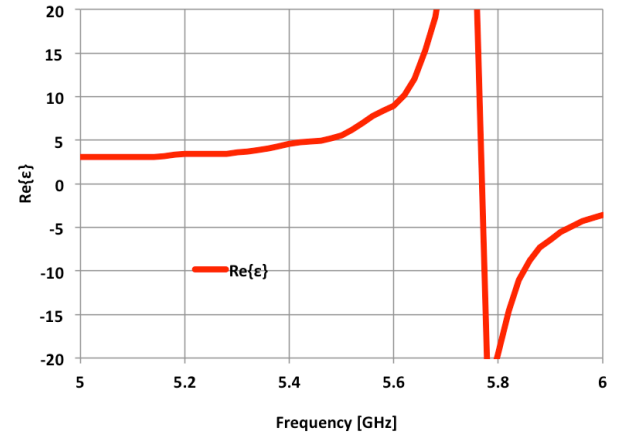


Fig. 6. Extracted permittivity for prototype electric disk resonator (EDR). Solid red line is real part of the effective permittivity $\text{Re}(\epsilon_r)$. Permittivity becomes negative above resonance frequency $\omega_e = 5.8$ GHz, as predicted in (7), when the denominator $\omega_e^2 - \omega^2$ is a small negative number.

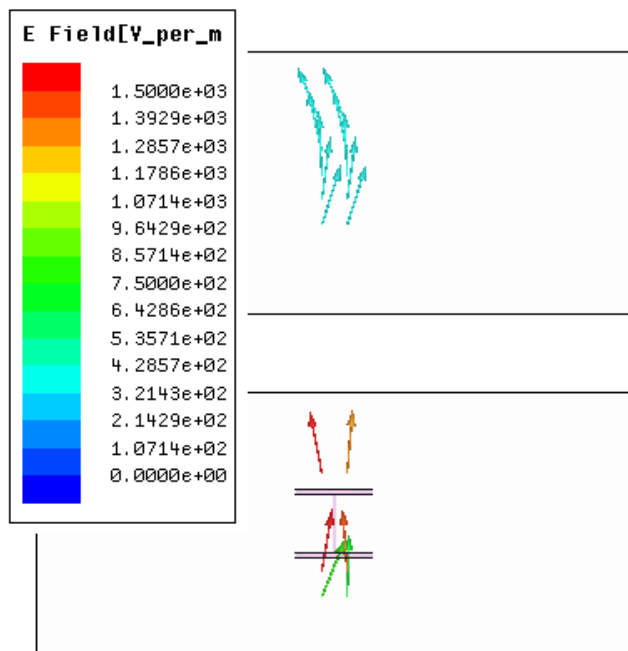


Fig. 7. Electric field simulation of EDR unit cell of Fig. 2 showing the field above the top disk and below the bottom disk at 5.7 GHz, just below the 5.8 GHz resonant frequency the EDR. Upper right box shows upward arrows in cyan color indicating an incident electric field at approx. 430 V/m. Lower right box shows EDR with red arrows indicating a upward total field of 1500 V/m. Other surrounding fields were cropped, boundaries are radiation boundaries. Incident wave propagation is from left to right.

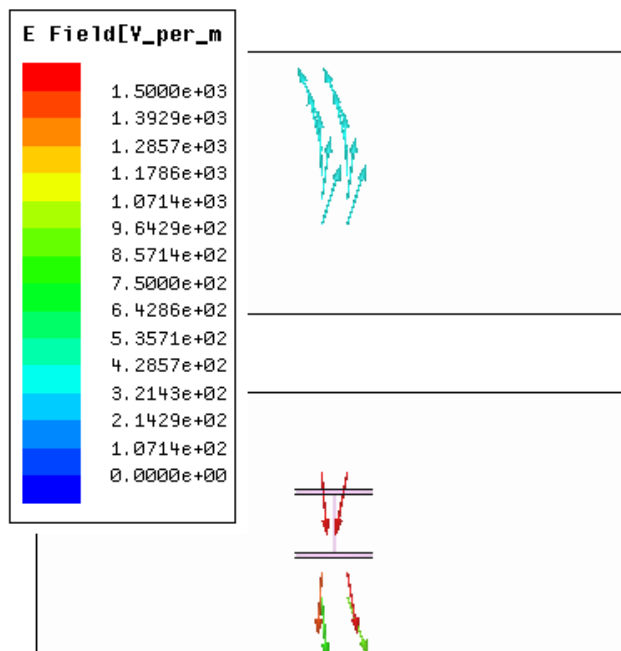


Fig. 8. Electric field simulation of EDR unit cell of Fig. 2 showing the field above the top disk and below the bottom disk at 5.9 GHz, just above the 5.8 GHz resonant frequency the EDR. Upper right box shows upward arrows in cyan color indicating an incident electric field at approx. 430 V/m. Lower right box shows EDR with red arrows indicating a downward total field of 1500 V/m. Other surrounding fields were cropped, boundaries are radiation boundaries.

ACKNOWLEDGMENT

This material is based upon work supported by the National Science Foundation under Grant No. ECCS-1101939.

REFERENCES

- [1] V. Veselago, "The electrodynamics of substances with simultaneously negative values of epsilon and mu," *Sov. Phys. Usp.*, vol. 10, pp. 509–514, 1968.
- [2] A. Lai, T. Itoh, and C. Caloz, "Composite right/left-handed transmission line metamaterials," *IEEE Microw. Mag.*, vol. 5, no. 3, pp. 34–50, Sep. 2004.
- [3] J. B. Pendry, A. J. Holden, W. J. Stewart, and I. Youngs, "Extremely low frequency plasmons in metallic mesostructures," *Phys. Rev. Lett.*, vol. 76, no. 25, pp. 4773–4776, Jun. 1996.
- [4] D. R. Smith, W. J. Padilla, D. C. Vier, S. C. Nemat-Nasser *et al.*, "Composite medium with simultaneously negative permeability and permittivity," *Phys. Rev. Lett.*, vol. 84, no. 18, pp. 4184–4187, May 2000.
- [5] T. Weldon, R. Adams, and R. Mulagada, "A novel unit cell and analysis for epsilon negative metamaterial," in *Southeastcon, 2011 Proceedings of IEEE*, Mar. 2011, pp. 211–214.
- [6] R. Ziolkowski, "Design, fabrication, and testing of double negative metamaterials," *IEEE Trans. Antennas Propag.*, vol. 51, no. 7, pp. 1516–1529, Jul. 2003.
- [7] A. Saha and M. Charise, "Effective permittivity of artificial material composed of metal particles -a generalized picture," in *Southeastcon, 2011 Proceedings of IEEE*, Mar. 2011, pp. 215–219.
- [8] J. Pendry, A. Holden, D. Robbins, and W. Stewart, "Magnetism from conductors and enhanced nonlinear phenomena," *IEEE Trans. Microw. Theory Tech.*, vol. 47, no. 11, pp. 2075–2084, Nov. 1999.
- [9] E. Poutrina, S. Larouche, and D. R. Smith, "Parametric oscillator based on a single-layer resonant metamaterial," *Optics Communications*, vol. 283, no. 8, pp. 1640–1646, 2010.

- [10] H. Mosallaei and K. Sarabandi, "Design and modeling of patch antenna printed on magneto-dielectric embedded-circuit metasubstrate," *IEEE Trans. Antennas Propag.*, vol. 55, no. 1, pp. 45–52, Jan. 2007.
- [11] J. T. Aberle, D. A. Buchanan, and W. E. McKinzie III, "Simulation of artificial magnetic materials using lattices of loaded molecules," *Proc. SPIE*, vol. 3795, pp. 188–196, Jul. 1999.
- [12] G. Donzelli, A. Vallecchi, F. Capolino, and A. Schuchinsky, "Metamaterial made of paired planar conductors: Particle resonances, phenomena and properties," *Metamaterials*, vol. 3, no. 1, pp. 10–27, 2009.
- [13] J. Barroso and U. Hasar, "Resolving phase ambiguity in the inverse problem of transmission /reflection measurement methods," *Journal of Infrared, Millimeter and Terahertz Waves*, vol. 32, pp. 857–866, 2011.
- [14] Z. Szabó and G.-H. Park, R. Hedge, and E.-P. Li, "A unique extraction of metamaterial parameters based on kramers-kronig relationship," *IEEE Trans. Microw. Theory Tech.*, vol. 58, no. 10, pp. 2646–2653, Oct. 2010.